JOURNAL OF AIRCRAFT
Vol. 33, No. 2, March–April 1996

Computational and Experimental Investigation of F/A-18E Sting Support and Afterbody Distortion Effects

R. H. Bush,* D. W. Jasper,† S. L. Parker,‡ W. W. Romer,§ and P. G. Willhite¶
McDonnell Douglas Corporation, St. Louis, Missouri 63166-0516

The F/A-18E/F program has recently completed a computational fluid dynamics (CFD) and experimental effort to determine sting and distortion increments for developing a preflight aerodynamic database. The CFD study provided pretest predictions of sting and distortion increments that supported initial performance predictions and directly contributed to the successful achievement of F/A-18E program goals. The study also produced quantitative pressure drag predictions for the F/A-18 wind-tunnel model at transonic conditions. Extreme fidelity in modeling the test article and care in the execution of the CFD solutions produced high-quality results that were validated by excellent agreement with the subsequent test results.

Introduction

THE single-place F/A-18E and two-place F/A-18F are significant upgrades to the current U.S. Navy F/A-18C/D Hornet fighter, offering increased range and payload while retaining the multimission fighter/attack capability that characterizes the F/A-18C/D. Major aerodynamic improvements on the F/A-18E/F include a larger wing and leading-edge extension, increased fuselage length, and larger horizontal and vertical tails. The F/A-18E/F has recently passed a significant program milestone by successfully completing its critical design review (CDR), signifying that the program is on schedule and ready for initial production.

Aerodynamic configuration development of the F/A-18E was supported by extensive testing of a 5% scale, sting-supported model. To account for the effects of the aft-mounted sting and its associated afterbody distortion, limited sting and distortion corrections were obtained using CFD methods. To support CDR, a new high-fidelity 8% scale model was constructed to perform aerodynamic database documentation testing. Because of a different sting installation and afterbody distortion, new sting and distortion corrections were required for the 8% model. Extensive sting and distortion corrections for the 8% model were to be obtained by testing a 15% scale pressure model, which would combine sting and distortion and jet effects testing (Fig. 1 and Ref. 1). However, testing of the 8% force model preceded testing of the 15% scale sting and distortion/jet effects model by several months, and early incorporation of the 8% model data into the aerodynamic database was given a high priority in supporting CDR. Therefore, a CFD study was initiated to provide predictions of sting and distortion increments at a limited number of flight conditions until the test data became available.

Model Design

The sting and distortion corrections to the 8% scale F/A-18E force model were to be obtained by testing a 15% scale pressure-instrumented model. A thorough study of available test techniques led to a joint recommendation by the organizations involved for the design of the sting and distortion/jet effects model. The design featured a wingtip support system as shown installed in the tunnel in Fig. 1. High-pressure air for simulating jet flows was delivered to the model through the wingtip mounting system. Pressure integration rather than a strain gauge balance was selected for increased measurement accuracy of afterbody force and moment increments. A model scale of 15% was selected to provide sufficient internal volume for the required onboard pressure instrumentation modules and air supply lines while providing acceptable wind-tunnel wall interference.

The model featured interchangeable distorted and real afterbodies for sting and distortion testing. All components forward of the afterbody were common to both configurations. The distorted afterbody configuration was a scaled representation of the 8% force model, including simulated flow through ducts, duct rakes, sting cavity, and dummy sting (Fig. 2). The real afterbody was representative of the F/A-18E aircraft, including variable exhaust nozzle geometry and nozzle pressure ratio (NPR) control for jet effects testing. The real afterbody also included simulation of the environmental control system (ECS) heat exchanger exhaust and engine bay vent (EBV) exhausts (Fig. 3), each with independent flow control. For the purpose of defining the sting and distortion increment, testing was con-

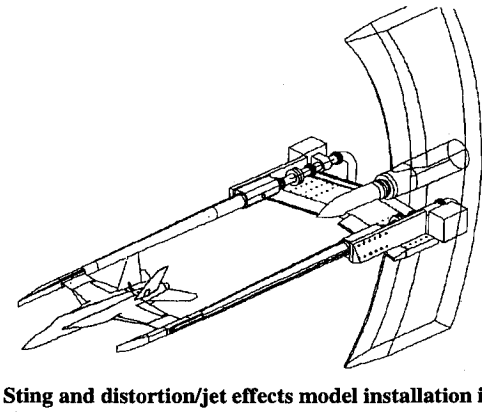

Fig. 1 Sting and distortion/jet effects model installation in AEDC 16T wind tunnel.

Presented as Paper 95-1779 at the AIAA 13th Applied Aerodynamics Conference, San Diego, CA, June 19–22, 1995; received Aug. 6, 1995; revision received Dec. 2, 1995; accepted for publication Dec. 2, 1995.

*Senior Principal Technical Specialist, Propulsion and Thermodynamics Department, CFD Project. Associate Fellow AIAA.

†Senior Project Engineer, Aerodynamics Department, F/A-18 Program.

‡Unit Manager, Aerodynamics Department, F/A-18 Program.

§Project Engineer, Propulsion and Thermodynamics Department, CFD Project.

¶Senior Project Engineer, Propulsion and Thermodynamics Department, CFD Project.

ducted with pressure-instrumented flush covers in place of the ECS and EBV exhausts.

The influence of control surface position on sting and distortion effects was an important test objective. Deflectable wing leading-/trailing-edge flaps and horizontal tail were incorporated into the design. The horizontal tails (stabilators) and vertical tails were common to the real and distorted afterbodies. Early in the design stage, concern arose over the ability to successfully integrate pressures on the deflectable horizontal tail. Consequently, the left-hand tail was instrumented with a strain gauge balance that subsequently confirmed the accuracy of pressure integration on the right-hand pressure-instrumented tail.

CFD results were used to determine the proper number and concentration of pressure taps required to accurately measure the changes because of sting and distortion effects over the range of test conditions. Approximately 1050 pressure taps were distributed over the external surface of the model, as illustrated in Fig. 4. Pressure taps were concentrated in the afterbody region where sting and distortion and jet effects are most pronounced. A sparse distribution of taps was included on the forward portion of the model to provide a closed body for pressure integration and minimize the effect of pressure instrumentation system bias on the results.

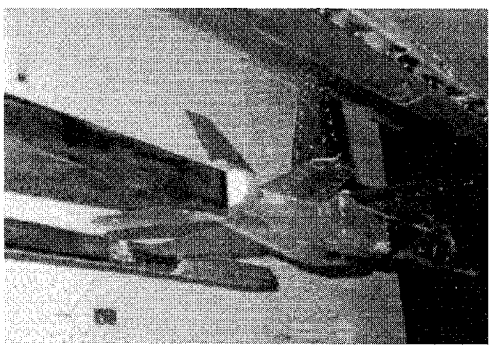

Fig. 2 Distorted afterbody with dummy sting.

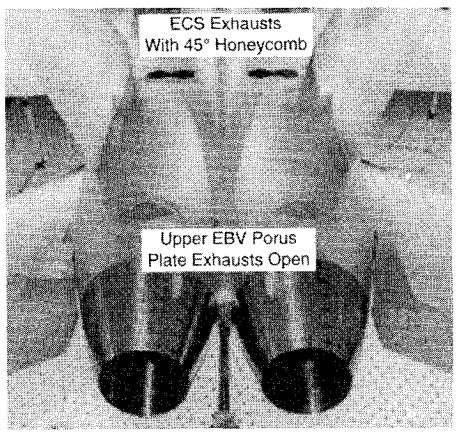

Fig. 3 Real afterbody configured with ECS and EBV open.

Several ancillary CFD studies were performed to support the wind-tunnel model design effort. Euler analyses were conducted to aid the design of an inlet fairing that would not impact the sting and distortion increments. This inlet fairing was then used in all subsequent computational and experimental studies. A Euler CFD study was used to ensure that the design of the support booms and their wingtip integration did not influence sting and distortion increments.

CFD Study

Since sting and distortion increments were required before the expected completion of the sting and distortion testing, a CFD study was initiated to provide pretest predictions. The predictions of the CFD study would be verified by comparison with the test results. Great care was taken to ensure that the geometry and flow conditions of the CFD study matched the proposed wind-tunnel test conditions to ensure that valid comparisons could be drawn. The wind-tunnel walls and model support system were included in the CFD analysis to improve the CFD-to-test comparison. As an added condition, to support F/A-18E/F program schedules, all CFD analyses were to be completed before entry of the model into the wind tunnel, limiting the computational portion of the effort to five months duration. The limited computational run matrix shown in Fig. 5 was defined as an achievable effort that provided increments at enough flight conditions to provide a meaningful database. This matrix represents 16 CFD cases, 8 flight conditions × 2 configurations (real and distorted).

To ensure that geometric ambiguities would not surface as potential causes of disagreement between the computed and measured data, the geometry for the CFD model was obtained from the same CAD database used to fabricate the wind-tunnel model. The CFD model included nearly all aspects of the wind-tunnel model, including the wingtip mounting system, inlet fairing, centerbody missile fairing, a missile fin cutout in the wing root trailing edge, horizontal and vertical tails, flowing nozzle, aft-facing nozzle base area, dummy sting, and the arresting hook fairing. The geometric compromises made were generally minor. The most significant were, control surface trailing edges were sharpened, the nozzle base was modeled

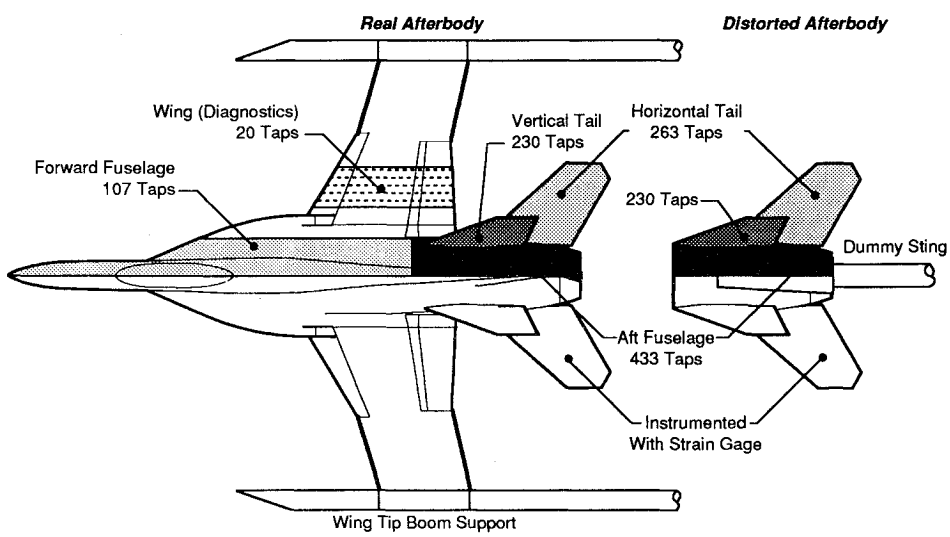

Fig. 4 Pressure tap distribution.

as a flat surface, the sting cavity was modeled as an aft-facing step, and the gap between the horizontal tail and nozzle (which allows the nozzle flaps to move in response to throttle setting), was filled.

A representative view of the real afterbody surface grid is shown in Fig. 6. Note that only 10,000 of 140,000 surface points are shown for clarity. The inlet fairing and missile fairing can be seen in this figure. Closeup views of the real and distorted afterbody grids are given in Fig. 7, again, with only a sparse surface grid shown. The complete grids for both the real and distorted afterbodies contained approximately five million points divided among 60 zones.

The flow solver code employed for this study was the three-dimensional Navier–Stokes time dependent (NASTD) code (Ref. 2). This finite volume code uses an approximately factored implicit upwind scheme and Roe's flux difference splitting method in the calculation of explicit fluxes. A keyword-based input data file is employed to specify run parameters. Boundary conditions are defined in a pointwise manner for each computational boundary, permitting nonpoint-matched zone interfaces. To more accurately model the experiment, a porous wall boundary condition[3] was implemented in NASTD to simulate the porous wind-tunnel wall.

The run conditions were specified to match as closely as possible the expected run conditions. The freestream Mach number and angle of attack corresponded to critical sting and distortion database points. The pressure and temperature were chosen to match the experimental values and Reynolds number. The distorted nozzle exit conditions were chosen to match those obtained in the flow through performance test, and simulated in the sting and distortion testing. The real nozzle exit conditions were chosen to correspond to expected flight values. The Baldwin–Barth one-equation turbulence model was used to model turbulence.

		Mach Number				
		0.60	0.85	0.90	1.05	1.20
α	0°	X	X	X	X	X
	1°					X
	3.5°	X	X			

Fig. 5 F/A-18E sting and distortion run matrix.

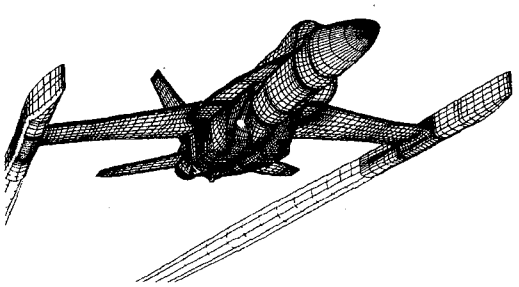

Fig. 6 Real afterbody surface grid.

A critical factor in completing this study in the allotted time frame was NASTD's newly implemented Parallel Virtual Machine (PVM) capability,[4] which allows the utilization of the collective power of a cluster of workstations for computing. Approximately 180 workstations, used as computer aided design (CAD) seats during daytime hours, were used in clusters of 10–15 per case for computational processing during off-shift hours. The PVM capability coupled with the large number of available workstations provided a major new resource to the F/A-18 project, allowing the expenditure of the equivalent of approximately 8000 supercomputer (200 Mflops sustained) CPU hours for this effort, in less than five months.

The primary convergence parameter monitored during each run was the integrated pressure drag on the surface of the model. For this purpose, all solid surfaces except the sting and internal nozzle surfaces were integrated. These pressure loads were tracked until the drag was converged to ±1 count ($C_d \pm 0.0001$). As an auxiliary check, the lift and pitching moment were also monitored. Each analysis required between 3000–12,000 iterations to meet the drag convergence criterion.

A standard set of plots was made for each of the solutions. These plots consisted of surface pressure contours (e.g., Fig. 8) and off-body cutting plane Mach and pressure contours to ensure that each solution had no discontinuities or nonphysical oscillations. Skin friction contour plots and particle traces were generated for selected cases to ensure that the boundary layers were well behaved. These plots also provided significant guidance in preparing for the wind-tunnel test. Regions of high flowfield gradients were identified, and the relevant physical behavior of the flow was noted. Also, by comparing the plots between various runs, the major flow features created by the distorted afterbody, as well as Mach and alpha effects, were identified.

Once a pair of real and distorted solutions was obtained, several checks were made to assess the quality of the drag increment. One was to project the distorted solution onto the real afterbody geometry, compute the difference of the pressures between the two, and plot surface contours of the incre-

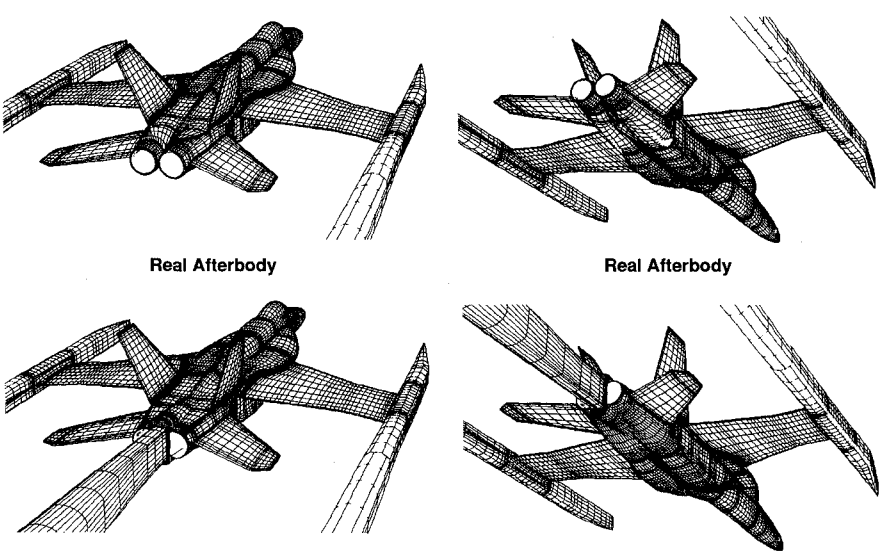

Fig. 7 F/A-18E 15% sting and distortion/jet effects model surface grid.

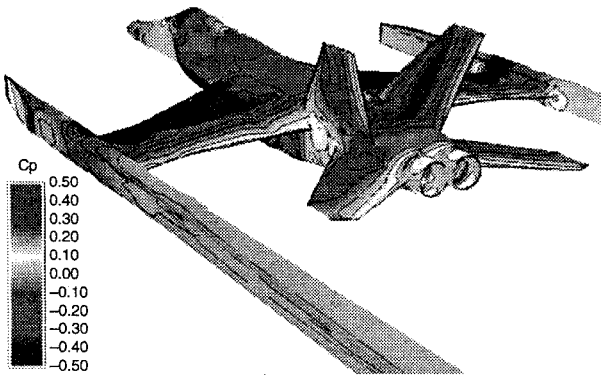

Fig. 8 F/A-18E, real aft end, booms, tunnel (Mach = 0.85, α = 3.5, Re = 3 × 10^6/ft, NPR = 6.40, surface pressure coefficient contours).

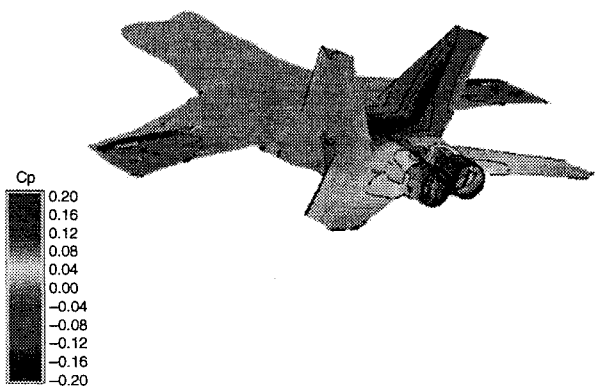

Fig. 9 F/A-18E, booms, tunnel (Mach = 0.85, α = 3.5, Re = 3 × 10^6/ft ΔC_p contours, real−distorted).

ment (Fig. 9). Note that the pressure scale is quite small and that the only significant difference between the solutions is in the afterbody region. This demonstrates the consistency of the independent real and distorted solutions in regions unaffected by the distortion. It also highlights the portion of the afterbody and tails affected by the distortion. Note that the comparison is most meaningful where the geometries are identical, in the distorted region, the pressure difference depends upon the projection algorithm used.

The CFD data were reduced using the same pressure integration coding as used in the test for generating force and moment data. This was done by interpolating the CFD solution data to the model pressure tap locations and performing a pressure integration using the areas defined on the model, ensuring consistency between the integrated CFD and experimental values.

The accuracy of the pressure integration employed on the test article was validated by the CFD results. The wind-tunnel model used for this study had over 1050 pressure taps, concentrated primarily in the afterbody region. By contrast, the CFD surface grid had well over 140,000 surface points, providing in effect a continuous pressure distribution. Thus, comparison of pressure integrations on the full CFD surface grid with those computed using only the pressure tap locations served to quantify the impact of finite tap resolution on the predicted increments. Note that the experimental pressure tap distribution was designed to predict afterbody drag increments, not absolute levels of full aircraft drag. The relatively coarse tap density on the forward fuselage of the model should not degrade the accuracy of the afterbody increment, even though the forebody drag is not well resolved. Indeed, while the difference in pressure drag between the full CFD surface grid integration and the tap integration ranged from 5 to 50 counts across the Mach/alpha range, the (real−distorted) pressure drag increment varied only between 0.1−2 counts.

The impact of the wingtip support booms and wind-tunnel walls on the sting and distortion increment was of particular interest to this study. Two additional solutions were performed without the support booms or wind-tunnel wall model (extending the CFD grid to model free air conditions) at Mach 0.85, α = 3.5. These solutions were then compared to the baseline cases to establish the combined impact of booms and wind-tunnel walls, two of the major differences that can impact wind tunnel to flight increments. While the presence of the wind-tunnel walls and support booms changed the predicted pressure drag by about seven counts, the predicted (real−dis-

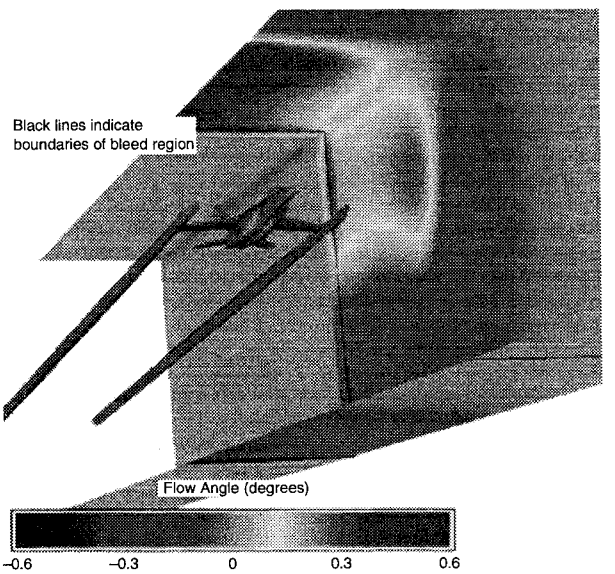

Fig. 10 F/A-18E, real aft end, booms, tunnel (Mach = 0.85, α = 3.5, Re = 3 × 10^6/ft, NPR = 6.397, flow angle relative to wall, positive into tunnel).

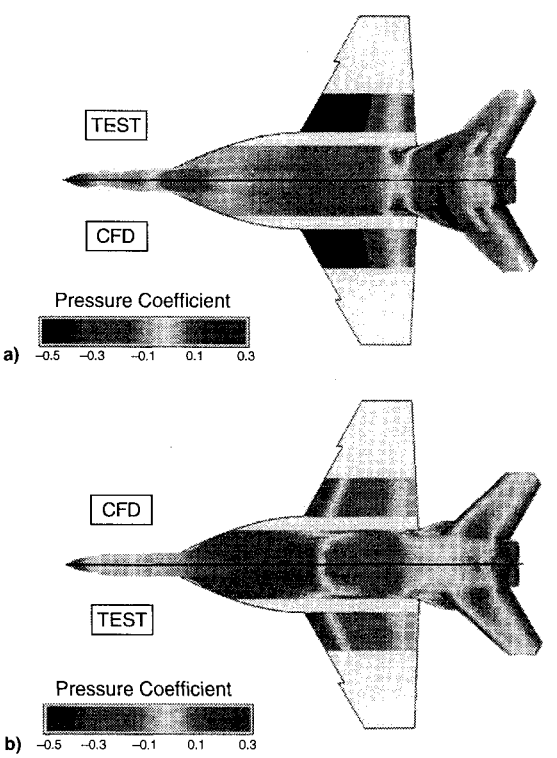

Fig. 11 Comparison of test and CFD predicted pressures: a) top and b) bottom views (F/A-18E sting and distortion model, real afterbody, Mach = 0.85, α = 3.5 deg).

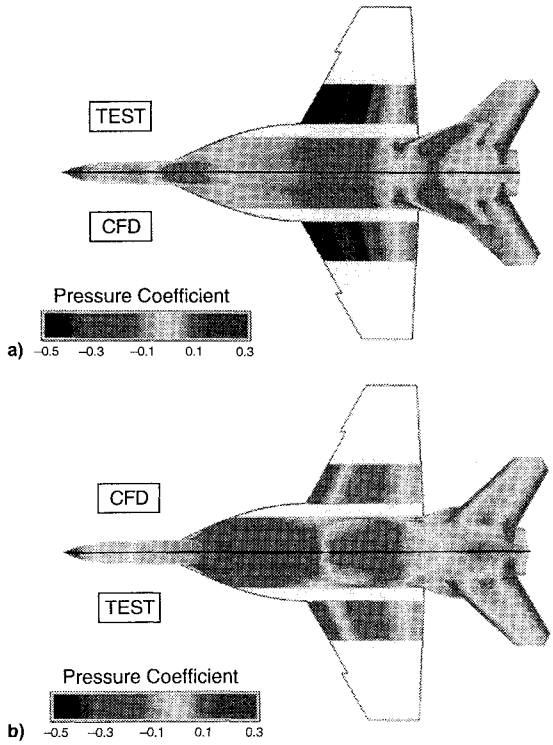

Fig. 12 Comparison of test and CFD predicted pressures: a) top and b) bottom views (F/A-18E sting and distortion model, distorted afterbody, Mach = 0.85, α = 3.5 deg).

torted) increment changed by less than 0.1 counts. The wall effects are illustrated in Fig. 10, which presents contours of outflow angle at the tunnel wall location. Note that the maximum outflow angle effected by the model was 0.6 deg.

The CFD results were also extremely useful in supporting the development of the on-site test support software. CFD pressures interpolated to the wind-tunnel model pressure tap locations were used to demonstrate and verify the test pressure integration software, three-dimensional color pressure display software, and on-line force and moment plotting and analysis software.

During the test, continuous on-line monitoring of pressures and integrated results was performed. Three-dimensional surface pressure color contour displays were monitored to assess data quality and support elimination and substitution of faulty pressure measurements as appropriate. On-line correlation of the pretest CFD predictions and test data led to high confidence throughout the test. CFD data were used to assess the impact of substitutions for faulty pressure measurements.

CFD/Test Comparisons

This study provided an excellent opportunity to assess the accuracy of the CFD results in replicating the experimental data. The dense pressure instrumentation on the model provided ample data to compare experimental and computed results in a direct manner. Also, because the CFD study was performed in conjunction with the wind-tunnel model development and test planning, geometry uncertainties were minimized, installation effects were modeled in the CFD, and data reduction was kept consistent. It is believed that these issues were major factors contributing to the excellent agreement to be shown.

Because of space constraints, results from only one set of flow conditions will be shown, Mach 0.85, α = 3.5. This case was chosen because it is a critical design point and one of the most difficult cases computationally. The results presented for this case are representative of those obtained throughout the present study. Additional and more detailed results can be found in Ref. 5.

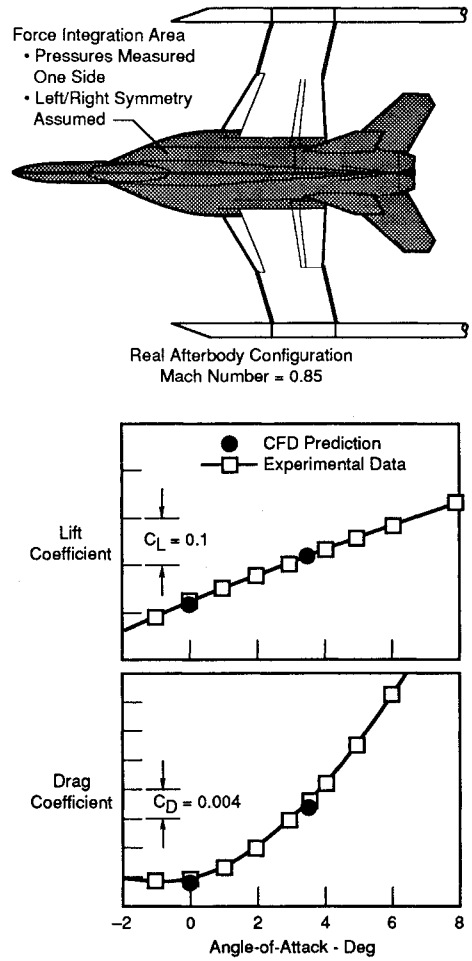

Fig. 13 Predicted and CFD drag polar predictions demonstrate quantitative accuracy.

Figures 11 and 12 show the surface pressure contours (plotted at the experimental tap locations) for the computational and experimental data, on the real and distorted afterbody configurations. There are no significant differences between computational and experimental data, which can be seen on this scale.

A more sensitive measure of the accuracy of the predicted surface pressures is a comparison of the integrated lift and drag from these pressures. Note that the pressure instrumentation was designed to obtain the difference in drag between the real and distorted geometries. Accurate measurement of the full configuration absolute force levels was not a test objective and would have required significant increases in tap density. However, comparison of the experimental and CFD lift and drag polars (Fig. 13) amply demonstrate the ability of CFD to provide quantitative pressure force predictions.

To show where the major contributors to the drag increment were generated, the distorted solution was projected onto the real geometry and the (real–distorted) pressures were plotted, as shown in Fig. 14 for both the computational and experimental results. This comparison also gives a sensitive means of locating small differences in the flowfields in undistorted regions. A few minor discrepancies in the level of contribution to the drag increment are evident between the CFD and test results, for example, on the aft fuselage above and below the horizontal tail. Generally, though, the contributors to the drag increment are well resolved by the calculation.

The final, and most important, measure of the accuracy of this study is a comparison of the computed and experimental force increments. Figure 15 shows the variation of the force increments with Mach number at 0-deg angle of attack and

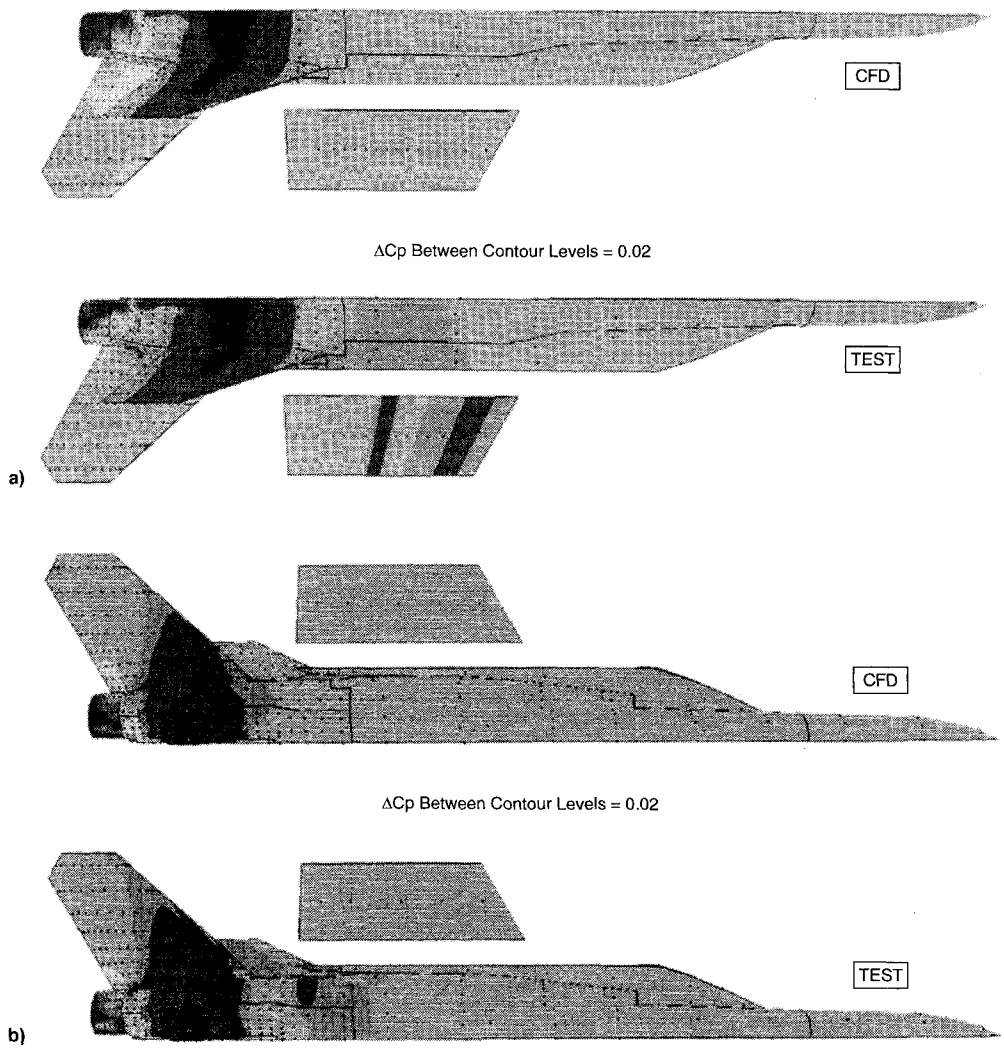

Fig. 14 Comparison of test and CFD (real–distorted) pressure differences: a) top and b) bottom views.

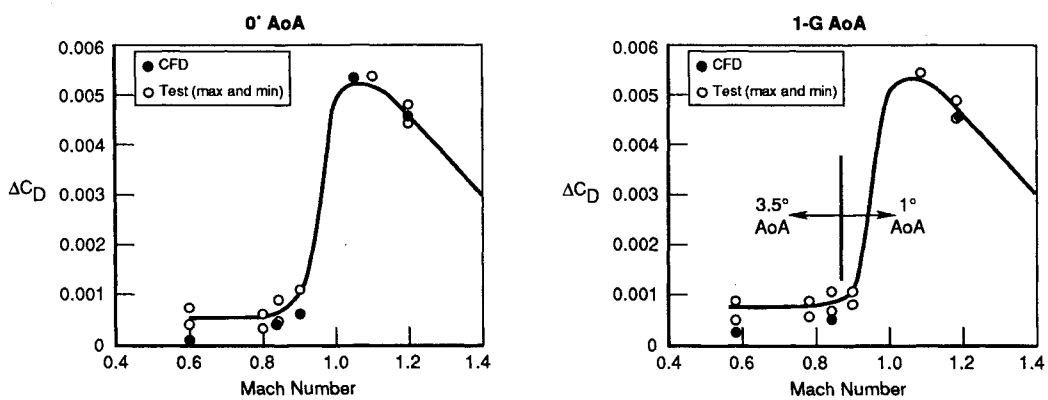

Fig. 15 Excellent agreement between test and CFD results (F/A-18E sting and distortion increment, $\Delta C_D = C_{D\,\text{real aft end}} - C_{D\,\text{distorted aft end}}$).

approximate 1-g flight conditions. Note that all of the CFD results represented were compiled before entry to the tunnel. The computed drag increment is lower than the experimentally determined drag increment at the lowest Mach condition. However, throughout the transonic and supersonic regimes, the predicted increment is within the experimental uncertainty. These comparisons demonstrate the ability of CFD to accurately predict the sting and distortion increments.

Conclusions

The F/A-18E/F program has completed a joint CFD and test program to generate sting and distortion increments for correcting a force model database. The CFD study satisfied the goal of predicting accurate sting and distortion increments and also provided excellent predictions of the absolute drag levels measured in the subsequent test. The CFD data were also used to reduce the risk of the wind-tunnel test by quantifying the impact of the pressure tap integration, wingtip support, inlet fairing, and wind-tunnel walls. CFD solutions provided insight into the flow phenomena associated with the model, and provided data for the development and testing of the wind-tunnel data reduction software. Test data provided validation of the CFD results and supplied the data necessary for completion of the performance database.

In this study, CFD demonstrated the ability to provide quantitative prediction of full aircraft drag increments in an aircraft development environment. This demonstrated the ability to deliver high-quality data in a timely manner, opening the door for greater utilization of CFD in supporting future aircraft development efforts.

Acknowledgments

As with any study of this size, there are numerous contributors. We would like to particularly thank the Sting and Distortion CFD Team at McDonnell Douglas Aerospace (MDA) who spent many hours producing the results presented here. We would also like to thank Naval Air Systems Command (NAVAIR), who provided the customer perspective; the CFD and experimental staff at the Arnold Engineering and Development Center (AEDC) for valuable recommendations on our approach; Northrop–Grumman (NG) for providing the geometry data for the wind-tunnel models; and the NG–MDA–AEDC–NAVAIR test crew, who spent many long hours acquiring the data.

References

[1]Miller, M. A., "Sting Distortion and Jet Effects Test of a 15-Percent Scale F-18E/F Model at Subsonic and Transonic Mach Numbers," Arnold Engineering and Development Center TSR-94-P10, Oct. 1994.

[2]Bush, R. H., "A Three-Dimensional Zonal Navier-Stokes Code for Subsonic Through Hypersonic Propulsion Flowfields," AIAA Paper 88-2830, July 1988.

[3]Martin, F. W., Jr., Sickles, W. L., and Stanley, S. A., "Transonic Wind Tunnel Wall Interference Analysis for the Space Shuttle Launch Vehicle," AIAA Paper 93-0420, Jan. 1993.

[4]Geist, A., Beguelin, A., Dongarra, J., Jiang, W., Manchek, R., and Sunderam, V., "PVM 3 User's Guide and Reference Manual," Oak Ridge National Lab., ORNL/TM-12187, Oak Ridge, TN, Sept. 1994.

[5]Willhite, P. G., Jasper, D. W., and Romer, W. W., "A Critical Evaluation of CFD Predictions of Full Aircraft Drag Increments," AIAA Paper 95-2289, June 1995.